RSC Advances

PAPER

View Article Online
View Journal | View Issue

Cite this: *RSC Adv.*, 2025, **15**, 49764

Engineering surface hydrophobicity/hydrophilicity of magnetic nanosorbents for efficient multipollutant water remediation

Akbar Mobaraki, *[a] Hani Paryabi,[ab] Mohsen Sheydaei*[b] and Fariborz Mansouri [c]

A series of magnetic sorbent materials were prepared *via* functionalization of magnetic nanoparticles using trimethoxymethylsilane (TMMS) and/or *N*-[3 (trimethoxysilyl)propyl]ethylenediamine (TMSPEDA) at varying molar ratios to precisely control surface hydrophobicity/hydrophilicity. The physic–chemical properties of the prepared materials were thoroughly elucidated by various techniques including Fourier-transform infrared spectroscopy (FT-IR), field emission scanning electron microscopy (FESEM), transmission electron microscopy (TEM), thermo-gravimetric analysis (TGA), vibrating-sample magnetometer (VSM), EDX and elemental mapping, wide-angle X-ray diffraction (XRD), N_2 adsorption/desorption analysis, and contact angle measurement, confirming successful modification and tailored surface properties. When evaluated for multipollutant water remediation, the optimized Mag@N1M3 exhibited superior performance in removing oils and organic pollutants due to its balanced hydrophobic/hydrophilic nature. Meanwhile, Mag@N1M1 showed exceptional efficiency in adsorbing trace Cr(VI) ions, attributed to its additional amine coordination sites. Thanks to their strong magnetic response, all sorbents were rapidly separated using an external magnet and reused for five cycles without significant efficiency loss, demonstrating excellent recyclability and potential for scalable water treatment applications.

Received 24th August 2025
Accepted 2nd December 2025

DOI: 10.1039/d5ra06301a

rsc.li/rsc-advances

Introduction

The exponential growth of global oil and petroleum industries has precipitated a parallel rise in catastrophic oil spill incidents, with an estimated 400 000 tons of oil discharged annually into aquatic ecosystems. The environmental devastation is exemplified by the Niger Delta, where over 1.5 million tons of crude oil has accumulated over decades, causing irreparable ecological damage.[1–5] Alarmingly, the World Wide Fund for Nature (WWF) warns that even two decades may be insufficient to remediate the aftermath of a major spill, underscoring the persistent nature of hydrocarbon contamination. Beyond large-scale disasters, chronic pollution from industrial discharges, food oils, and domestic wastewater further exacerbates this crisis, threatening marine biodiversity, disrupting ecosystems, and incurring staggering economic costs for remediation.[1–5] Therefore, finding urgent solutions for separation of spilled oil from water is a great challenge not only from the environment and economic viewpoints but also from the public concern view. Regularly, the removal of oil contamination from water usually accomplishes *via* two methods including burning and collecting. Conventional mitigation strategies, such as *in situ* burning, are increasingly untenable due to secondary pollutants and safety hazards. In contrast, mechanical recovery methods offer a sustainable alternative by enabling direct oil retrieval without generating additional contaminants. However, their efficacy hinges on the development of advanced sorbent materials engineered for high selectivity, capacity, and reusability. Addressing these challenges requires innovative design of highly efficient and task-specific sorbent material, where tuneable surface properties enable adaptive pollutant removal, bridging the gap between environmental needs and technological solutions.

In recent years, there has been a much growing attention to prepare new materials for efficient and selective elimination of varied oil and organic pollutants from water.[6–10] A wide variety of materials including wettable sorbents, polymeric and biopolymeric sorbents, biomimetic super-lyophobic and super-lyophilic sorbents, porous biodegradable sorbents, nanohybrid sponge sorbents, nanostructure and porous sorbents, different transition metal and metal oxide sorbents, metal–organic frameworks, and various allotrope of carbon based sorbents, *etc*, have been employed for such application.[11–20] Despite their significant achievements in both academic and industry, there are some intrinsic difficulties associated with these compounds such as difficulty in collecting and managing owing to their small particle size (usually ultra-filtration or

[a]*Department of Organic and Polymer Chemistry, Faculty of Chemistry, Kharazmi University, P. O. Box: 15719-14911, Tehran, Iran. E-mail: akbar.mobaraki@khu.ac.ir*
[b]*Department of Applied Chemistry, Faculty of Chemistry, Kharazmi University, P. O. Box: 15719-14911, Tehran, Iran. E-mail: Mohsen_sheydaei@khu.ac.ir*
[c]*Department of Chemical Technologies, Iranian Research Organization for Science and Technology (IROST), Tehran, Iran. E-mail: f.mansouri@irost.ir*

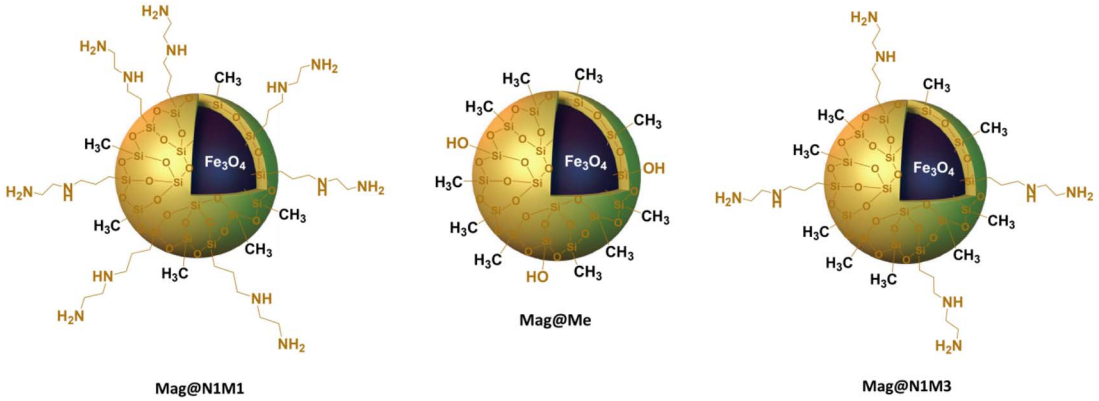

Fig. 1 Schematic representation of the magnetic hydrophobic/hydrophilic Mag@Me, Mag@N1M3, and Mag@N1M1 sorbents.

centrifugation is necessary), regeneration at high temperatures such as about 800 °C for activated charcoal, tedious and complex recovery processes and low separation efficiency. In addition, common polymeric sorbents suffer from decomposition at elevated temperatures and lack of inherent selectivity. To overcome these limitations, recently, the use of magnetic nanoparticles (MNPs) or nanocomposites as an alternative for traditional sorbents has received substantial interest because of their sufficient specific surface area, high adsorption capacity as well as easy and targeted functionalization for enhance selectivity towards the desired analytes.[21,22] Most importantly, the capability to simple and quickly separate MNPs using an external magnet simplifies the recovery and reuse of the sorbent to a great extant. Among the various types of MNPs, magnetite (Fe_3O_4) nanoparticles are the most favourable explored magnetic materials due to their readily accessibility from commercially available starting materials, low toxicity and superparamagnetic behaviour. Along this line, a wide variety of bare or functionalized MNPs or their nanocomposites have been used successfully for the separation of oil from water.[23–27] While acknowledging their achievements in the development of magnetic nanomaterials for oil separation technology, a fundamental scientific challenge in the design of magnetic sorbents remains inadequately addressed: the balance between surface hydrophobicity and aqueous dispersibility. There is still need to more discover about the relationship between the surface chemistry of MNPs and their oil separation efficiencies. Conventional strategies predominantly focus on developing highly hydrophobic or superhydrophobic surfaces to enhance oil affinity.[28–30] However, such surfaces often lead to the aggregation and precipitation of MNPs in water. This aggregation drastically reduces the effective surface area accessible to oil droplets, thereby diminishing separation efficiency. The ideal magnetic sorbent must, therefore, achieve a delicate balance: it must be hydrophobic enough to capture oil, yet sufficiently hydrophilic to remain well-dispersed in the aqueous phase to ensure full accessibility to water contaminators. In other words, thanks to MNPs nano-metric dimensions, although MNPs are well-dispersed in numerous solvents, they cannot afford a suitable exposure of their active surfaces in the proximity of organic pollutants when water is the reaction medium. Consequently, tuning the hydrophilic and hydrophobic character at the surface of MNPs or nanocomposites in the design of highly efficient and task-specific magnetic sorbents for separation of oil from water is a key problem that should be resolved. This issue has been less investigated in the previous studies on the development of magnetic sorbents for oil separation.[31,32] To address this limitation, herein, we reported on the hydrophilic/hydrophobic character adjustment in the surface of MNPs to improve their concomitants dispersion in aqueous medium as well as their interaction with oil contaminations thus to enhance the oil separation efficiencies. To do this, silica-coated iron oxide MNPs were functionalized with various functional organic compounds such as trimethoxymethylsilane (TMMS) and *N*-[3 (trimethoxysilyl)propyl]ethylenediamine (TMSPEDA) with varied molar ratio to tune the hydrophilic/hydrophobic character of the surface. In other words, the unique advantage of this approach lies in the active regulation of the TMMS/TMSPEDA ratio, which allows for systematic control over the hydrophilic–hydrophobic balance. This goes beyond simply creating a hydrophobic sorbent; it enables the engineering of a task-specific material that maintains excellent dispersion in water (through TMSPEDA) while providing strong interaction with oil contaminants (through TMMS). This targeted surface engineering, which directly addresses the dispersibility challenge of highly hydrophobic sorbents, represents a significant advancement over previous studies that have largely overlooked the optimization of this balance. From another perspective, it might be said that extreme hydrophobicity alone does not maximize oil and organic pollutant adsorption. Purely hydrophobic surfaces tend to undergo stronger particle–particle interactions in water, leading to rapid aggregation and reduced effective dispersion. As a result, the number of accessible interfacial adsorption sites decreases, limiting contact with oil droplets. In contrast, creation of a balanced between hydrophobicity and hydrophilicity on the sorbent surface through the co-presence of nonpolar TMMS and polar TMSPEDA groups enhances the dispersal of the sorbent in the aqueous medium. Improved dispersion significantly enhances the probability of sorbent-oil collision events, increasing the adsorption rate and capacity. The hydrophobic domains promote strong van der Waals and interfacial interactions with nonpolar oils, while the

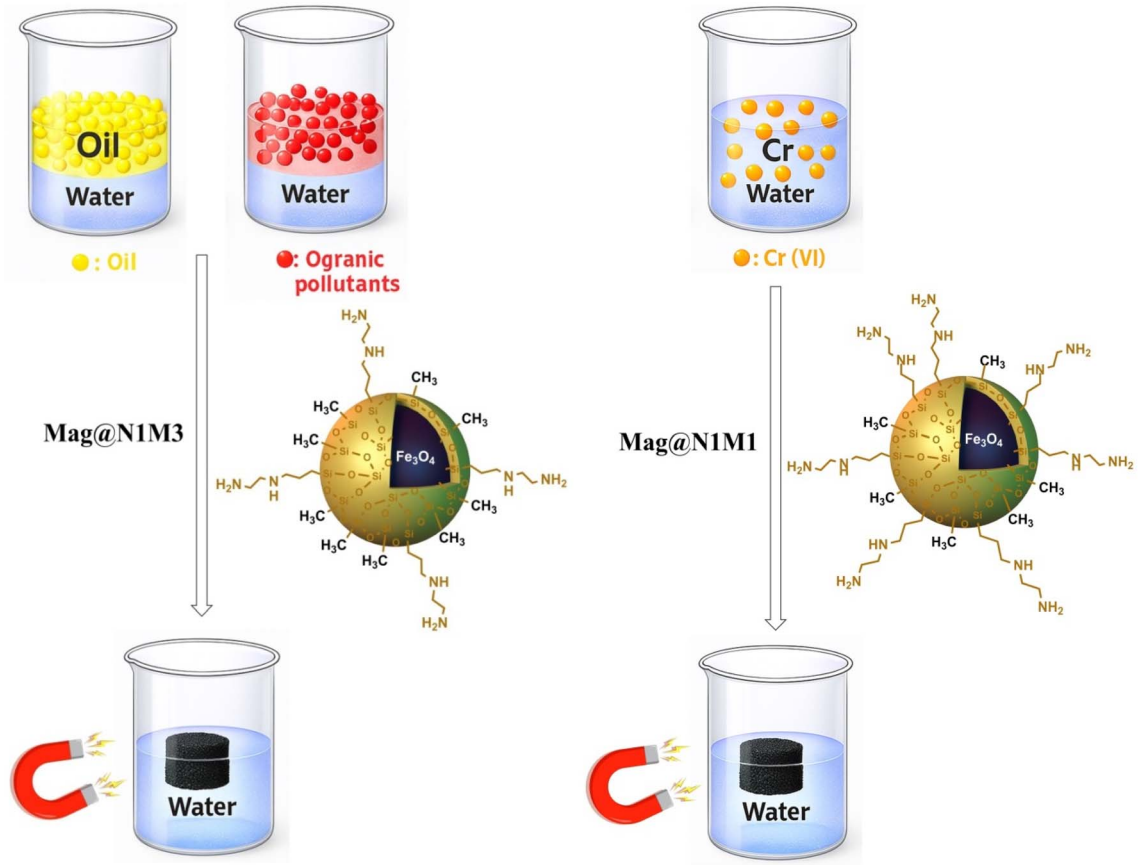

Fig. 2 Schematic representation of the magnetic separation of oil, organic and chromium ion contaminations from water.

hydrophilic sites maintain particle stability in water, preventing aggregation.

The prepared materials denoted as Mag@Me, Mag@N1M3, and Mag@N1M1 (Fig. 1) have investigated for the separation of oil and organic contaminations as well as chromium ion from water (Fig. 2).

Experimental

Materials and methods

Ferrous chloride tetrahydrate, ferric chloride hexahydrate, ammonia, tetraethyl orthosilicate (TEOS), TMMS, TMSPEDA, ethanol, *n*-hexane, methanol, acetonitrile, ethyl acetate, and acetone, with synthesis and analytical grades were provided from Sigma-Aldrich and Merck Co. Fourier transform infrared (FT-IR) spectra were acquired using a FT-IR spectrometer (PerkinElmer Spectrum RXI) at room temperature, with KBr discs. Transmission electron microscopy (TEM) images were captured by Philips EM 208S equipment. The X-ray diffraction (XRD) patterns were analyzed using a Philips PW1730 X-ray diffractometer equipped with Cu-Kα radiation. An Energy dispersive X-ray (EDX) analysis was carried out utilizing a TESCAN MIRA III analyzer, which is an environmental scanning electron microscope. The vibrating sample magnetometer (VSM) was utilized to calculate the magnetization curve of the magnetic samples by applying a 15 kOe magnetic field at room temperature. The thermal stability of the magnetic sorbents was examined by SDT Q600 V20.9 Build 20 Thermo-gravimetric Analyzer (TGA) in the temperature range of 0 to 800 °C.

The MIRA III – TESCAN device was used to conduct Field Emission Scanning Electron Microscopy (FESEM). The N_2 adsorption/desorption analysis was carried out in a Belsorp-mini-BEL Japan, Inc. at 298 K. An Avaspec-2048-TEC UV-vis spectrophotometer was used to evaluate the chromium(VI) removal efficiency.

Preparation of the magnetic sorbents

The preparation of Fe_3O_4 MNPs was accomplished *via* methods reported in the literature.[33] In this experiment, 4.0 g (20.1 mmol) of iron(II) chloride tetrahydrate ($FeCl_2 \cdot 4H_2O$) and 11.0 g (40.7 mmol) of iron(III) chloride hexahydrate ($FeCl_3 \cdot 6H_2O$) were dissolved in 250 mL of distilled water. The dissolution process took place under a nitrogen environment with a mechanical stirrer at 500 rpm and at a temperature of 85 °C. The pH of the solution was adjusted to the range of 9–11 by gradually adding 25% NH_3 aqueous solution dropwise. After undergoing continuous agitation for duration of 4 h, black magnetite nanoparticles (Fe_3O_4) were generated as a result of precipitation. The black deposited solid was rinsed multiple times with distilled water (5 × 100 mL) and then gathered using an external magnet. The silica-coated magnetic nanoparticles were synthesized by ultrasonically (40 kHz) pre-mixing a dispersion

of 2.0 g of Fe_3O_4 black precipitate in 400 mL of ethanol for about 30 min at 25 °C. Afterward, 12 mL of aqueous solution of NH_3 (25%) and TEOS (4.0 mL) were sequentially and gradually introduced at the same temperature. The solution obtained was agitated mechanically at 500 rpm for a continuous period of 24 h at a temperature of 25 °C. Following this, the Fe_3O_4@SiO_2 products were gathered using an ordinary magnet, rinsed with ethanol (3 × 25 mL), and left to dry using vacuum at 25 °C for the entire night. Ultimately, the process of modifying the surface of Fe_3O_4@SiO_2 core–shell MNPs with methyl group required a synthetic technique that utilized the grafting of TMMS onto the Fe_3O_4@SiO_2 core–shell MNPs. To achieve this objective, 0.4 g of TMMS (2.94 mmol) was introduced into 35 mL of anhydrous toluene that already contained Fe_3O_4@SiO_2 core–shell MNPs (1.0 g). The mixture was then agitated at 500 rpm for 24 h under reflux conditions. The magnetic sample obtained was rinsed multiple times with toluene (2 × 15 mL) and ethanol (3 × 25 mL). The appropriate magnetic Fe_3O_4–SiO_2@Me sorbent was obtained by drying it overnight at ambient temperature under vacuum (denoted as Mag@Me). The same procedure was employed for the synthesis of Fe_3O_4@SiO_2@-N1M3 (denoted as Mag@N1M3) in which Fe_3O_4@SiO_2 functionalized with both TMMS and TMSPEDA with molar ratio of 3 : 1. Also the procedure was applied for the synthesis of Fe_3O_4@SiO_2@N1M1 (denoted as Mag@N1M1) in which Fe_3O_4@-SiO_2 was anchored with equal molar ratio (1 : 1) of both TMMS and TMSPEDA.

General procedure for oil and organic pollutants separation using magnetic sorbents

The procedure for evaluating the oil adsorption capacity of magnetic sorbents was accomplished based on weight measurement. The appropriate amount of magnetic sorbent nanoparticles (0.07–0.1 g) was weighed as m_1. 0.5 g of oil or organic pollutants denoted as m_2 was mixed with 40 mL distilled water, and then magnetic sorbent was added to it and vigorously stirred at 800 rpm. The oil or organic pollutants were adsorbed by the magnetic sorbent during a few minutes (7 min, unless stated). Afterwards, the magnetic sorbent together with the adsorbed oil or organic pollutants were collected by nearing an external magnetic bar to the bottom of the reaction vessel and decanting the water. The collected particles was left for 24 h to evaporate any possible adsorbed water and then weighed as m_3 (refer to the SI for photos depicting the Experimental section of oil separation). Finally, the sorption capacity (Q) of nanoparticles was calculated by the following formula:

$$Q = (m_3 - \mathrm{m}_1)/m_2 \times 100$$

For the recovery test, magnetic sorbent nanoparticles were washed by acetone under ultrasonic irradiation (during 15 min and 40 kHz) for three times to completely remove the adsorbed oil then collected with a magnetic bar and dried in oven at 50 °C for 2 h to remove residual acetone. Then it was reused to separate oil from water for the next runs. All experiments were repeated for 3 times and the average data was reported.

General procedure for separation of chromium(VI) from aqueous medium using magnetic sorbents

Initially, 2 and 5 mg L^{-1} aqueous solutions of chromium(VI) were prepared *via* dissolving of appropriate amounts of $K_2Cr_2O_7$ in water. Then, 10 mL of light orange chromium(VI) solution was mixed with 0.05 g of each sorbent and stirred at room temperature using a shaker at 230 rpm during appropriate time. After the process, magnetic sorbent was separated with an external magnet and the remained solution was subjected to the analysis with spectrophotometer. Spectrophotometric measurement at 540 nm, in the presence of 1,5-diphenylcarbazide as indicator, was employed for the determination of chromium ion concentration before and after treatment with sorbents. To do this, 1,5-diphenylcarbazide solution was prepared *via* dissolving 0.5 g 1,5-diphenylcarbazide in 100 mL acetone followed by addition of 0.5 mL H_2SO_4 (0.5 N) to it. For the sample preparation, a 50 mL aqueous solution was prepared by mixing 5 mL of the chromium(VI) solutions (before or after treatment with sorbent) and 1 mL of 1,5-diphenylcarbazide solution. When these two are mixed in an acidic medium, a highly sensitive colorimetric reaction occurs. Chromium(VI) oxidizes 1,5-diphenylcarbazide to 1,5-diphenylcarbazone. Simultaneously, the chromium(VI) is reduced to chromium(III). The Cr(III) ions then immediately form a stable, soluble complex with the 1,5-diphenylcarbazone. This complex has an intense and characteristic violet colour. Supernatants and standard solution of chromium ion were analyzed at 540 nm with the spectrophotometer. Finally, the removal efficiency was obtained using the following formula:

$$\text{Removal efficiency (\%)} = (C_0 - C_\mathrm{f})/C_0 \times 100$$

In which, C_0 and C_f are initial and final concentration of chromium(VI) based on mg L^{-1}, respectively (refer to the SI for photos depicting the Experimental section of chromium(VI) separation).

Results and discussion

To prepare magnetic sorbent materials, initially iron oxide magnetic nanoparticles were prepared *via* known co-precipitation method employing Fe(II) and Fe(III) under basic environment and followed by surrounding the magnetic nanoparticles with silica shell through hydrolysis and condensation of TEOS, to give the desired core–shell Fe_3O_4@SiO_2 nanoparticles. Next, on the basis of our initial goal to prepare magnetic sorbents with varied surface hydrophilicity/hydrophobicity, three materials were prepared through functionalization of Fe_3O_4@SiO_2 nanoparticles with TMMS and TMSPEDA or both with different percent of functional groups under refluxing in dry toluene, as following: (i) Fe_3O_4@SiO_2@-Me (denoted as Mag@Me) which was prepared *via* functionalization of Fe_3O_4@SiO_2 only with TMMS, (ii) Fe_3O_4@SiO_2@N1M3 (denoted as Mag@N1M3) which was synthesized *via* functionalization of Fe_3O_4@SiO_2 with both TMMS and TMSPEDA employing 3 : 1 molar ratio, respectively, and (iii) Fe_3O_4@-SiO_2@N1M1 (denoted as Mag@N1M1) which was prepared *via*

anchoring Fe_3O_4@SiO_2 with equal molar ratio of both TMMS and TMSPEDA (Scheme 1).

In the next step, the physic–chemical properties of the prepared materials were thoroughly elucidated by various techniques including FT-IR, FESEM, TEM, TGA, VSM, EDX and elemental mapping, XRD, N_2 adsorption/desorption analysis, and contact angle measurement.

In order to effectively investigate the formation of chemical bonds and the presence of functional groups in the prepared materials, the Fe_3O_4 MNPs, Fe_3O_4@SiO_2 core–shell MNPs, and the magnetic sorbents including Mag@Me, Mag@N1M1 and Mag@N1M3 were studied using FT-IR spectroscopy (Fig. 3). As demonstrated in Fig. 3(a–e) the absorption band observed at about 598 cm^{-1} could be related to the stretching vibrations of the Fe–O–Fe bond in the pure Fe_3O_4.[34] Symmetric vibration of Si–O–Si at about 475 and 967 cm^{-1} and asymmetric vibration of this bond at about 1096 cm^{-1} strongly support the formation of silica shell around the iron oxide core in the materials (Fig. 3b–e).[34] The observation of a weak band at about 816 cm^{-1} which indicates the presence of Si–O–Fe bond, as well as the existence of surface Si–O–H vibrations above 3000 cm^{-1} are supplementary confirmations for the presence Fe_3O_4@SiO_2 phase in the developed materials. Additionally, the strong vibration of aliphatic C–H bonds at about 2937 and 2867 cm^{-1} and the bending vibration of this bond at about 1491 cm^{-1} as well as stretching vibration of N–H bond at about 3431 cm^{-1} and the bending vibration of this bond at about 1645 cm^{-1}, strongly identified the functionalization of support with TMMS and/or TMSPEDA (Fig. 3c–e).[35] The XRD pattern of Fe_3O_4 nanoparticles along with the Mag@Me, Mag@N1M1 and

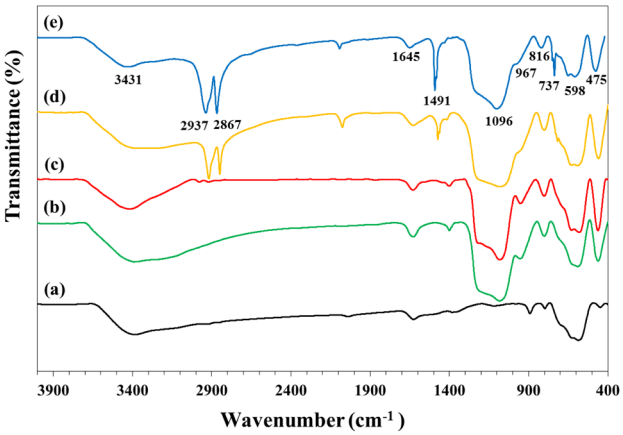

Fig. 3 FT-IR spectra for Fe_3O_4 (a), Fe_3O_4@SiO_2 (b), Mag@Me (c), Mag@N1M1 (d) and Mag@N1M3 (e). To see single and large spectrum, refer to SI.

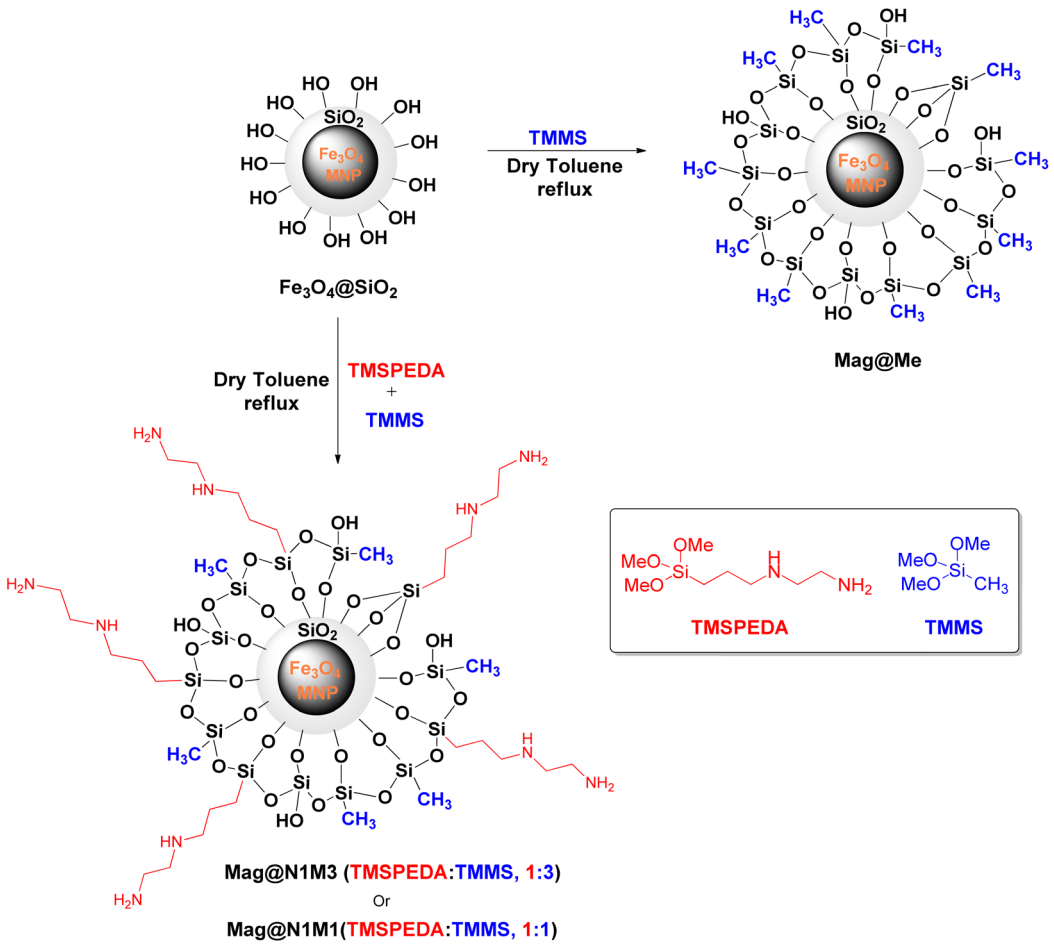

Scheme 1 Synthetic route for Mag@Me, Mag@N1M3, and Mag@N1M1.

Mag@N1M3 sorbents was examined to identify their crystalline structure and phase purity (Fig. 4). The Fe_3O_4 nanoparticles exhibited diffraction peaks at 2θ values of 30.2, 35.5, 43.2, 53.5, 57.2 and 62.8°, which completely matched with (220), (311), (400), (422), (511) and (440) crystallographic planes of Fe_3O_4 MNPs, respectively. This confirms the inverse spinel cubic structure of magnetite (JCPDS file no. 088-0315).[34]

Almost similar diffraction patterns were also observed for Mag@Me, Mag@N1M1 and Mag@N1M3 sorbents with slightly lower sharpness as evidence for successful surrounding of iron oxide core with the silica as well as organic functional groups. However, all sorbents have still demonstrated distinct and sharp peaks indicating their high crystallinity even after functionalization process. In other words, the surface modification process did not alter the core crystalline phase of the Fe_3O_4 nanoparticles. The full width at half maximum of the most intense diffraction peak at 2θ value of 35.5 matched with (311) crystallographic plane remains largely unchanged across all samples. This suggests that the functionalization process occurred on the surface without causing significant dissolution/recrystallization of the magnetite core. In addition, a noticeable increase in the background hump in the 2θ range of 15–30° is observed for the Mag@Me, Mag@N1M1 and Mag@N1M3 sorbents compared to the pristine Fe_3O_4. This is attributed to the presence of an amorphous silica and organic layer deposited on the surface of the crystalline nanoparticles.[35] No additional peak was observed in the XRD pattern of sorbents confirming the high phase purity of the prepared materials. These findings collectively confirm the successful formation of a core–shell structure where a crystalline Fe_3O_4 core is preserved, and an amorphous silica and organic shell is grafted onto its surface.

FESEM images of the prepared Mag@Me, Mag@N1M1 and Mag@N1M3 sorbents at different magnifications demonstrated that the material composed of uniform spherical nanoparticles with narrow particle size distribution almost in the range bellow 80 nm (Fig. 5).

To achieve more deep and comprehensive view on the particle size and textural structure, iron oxide nanoparticles and all sorbents were subjected to TEM analysis. Fe_3O_4 nanoparticles demonstrated uniform and spherical morphology with narrow size-distribution.

The TEM images of the sorbent materials were also confirmed the uniform particle size distribution of the all material, in agreement with the FESEM images, as well as their core–shell structure, which was preserved even after functionalization with organic moieties. The silica layer may be visually identified as bright areas surrounding the dark Fe_3O_4 MNPs in the TEM images (Fig. 6).

The chemical composition and elemental distribution of the prepared Mag@Me, Mag@N1M3, and Mag@N1M1 magnetic sorbents were quantitatively assessed using EDX analysis as well as elemental mapping (Fig. 7–9). The EDX analysis indicated distinct peaks for all O, Si, Fe, N and C expected elements, as verification for the presence of iron oxide core, silica shell and successful attachment of the TMMS and TMSPEDA onto the surface of the all materials.

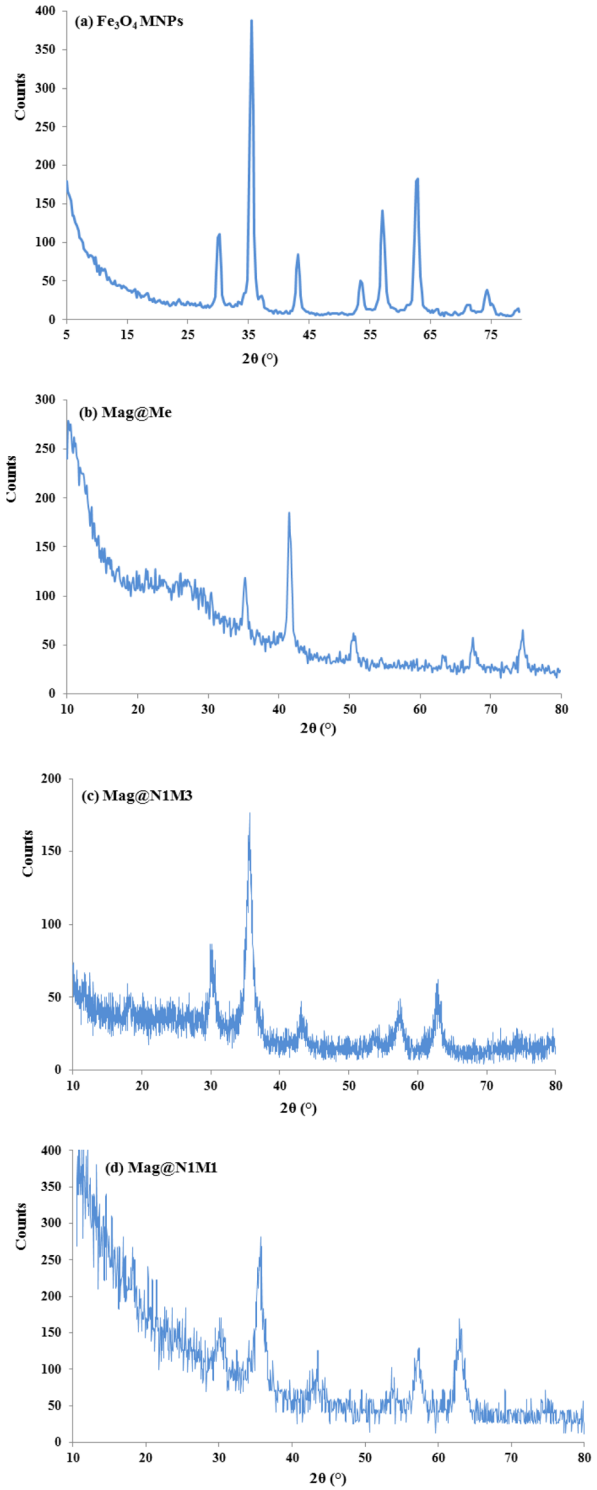

Fig. 4 XRD patterns of (a) Fe_3O_4 MNPs, (b) Mag@Me, (c) Mag@N1M3, and (d) Mag@N1M1. To see large pattern, refer to SI.

The quantitative findings from the EDX analysis are shown in the Fig. S37–S39 within the SI. The high atomic percentage of carbon (40.57%) in the Mag@Me magnetic sorbent confirms the successful grafting of TMMS onto the Fe_3O_4 magnetic core which is responsible for the significant hydrophobicity of the sorbent. This grafted organic layer forms a non-polar surface,

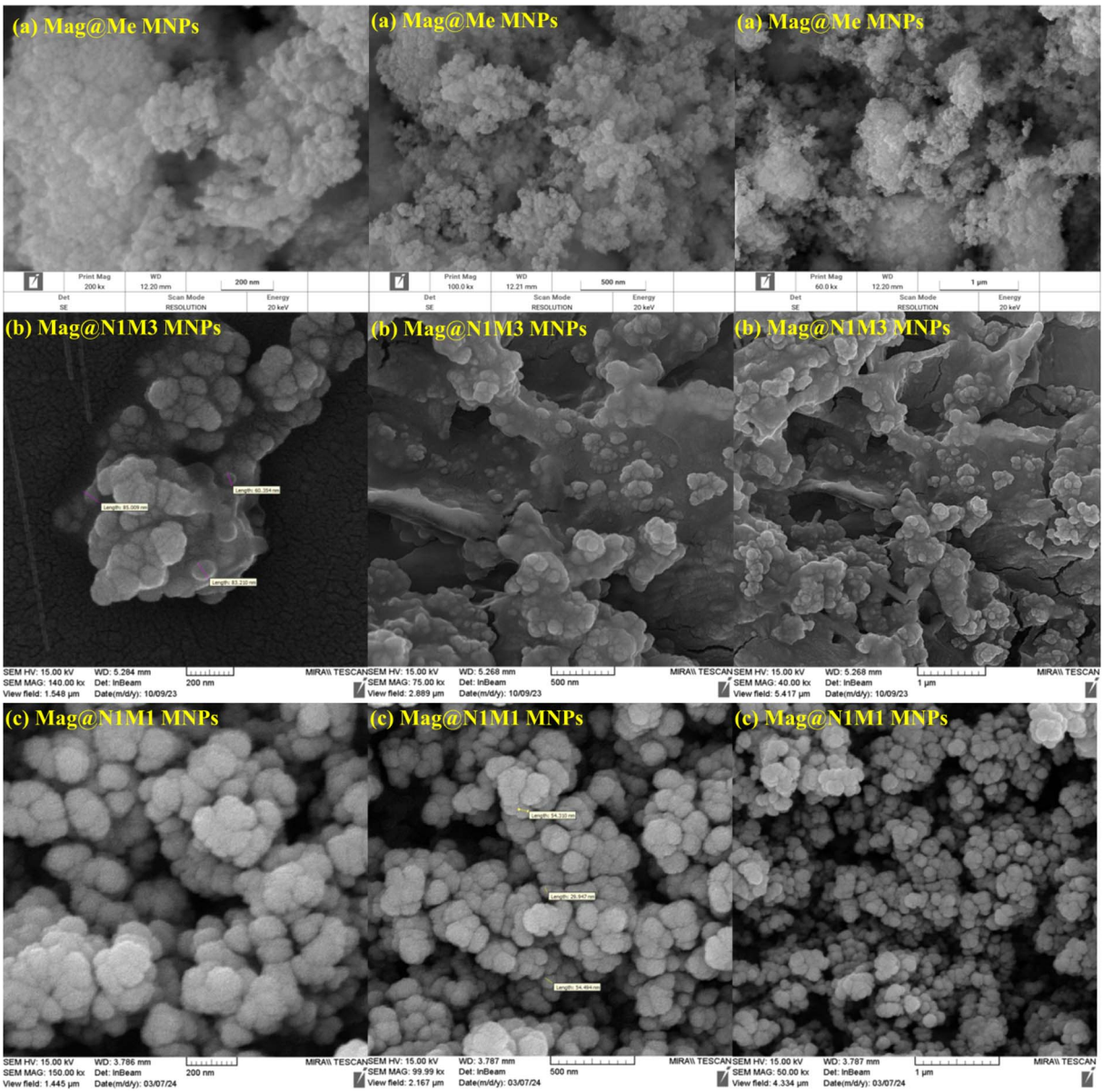

Fig. 5 FESEM images of (a) Mag@Me, (b) Mag@N1M3, and (c) Mag@N1M1 in three: 200 nm, 500 nm and 1 μm magnifications. To see large images, refer to SI.

thus improving its preference for hydrophobic interactions. The successful co-grafting of both TMMS and TMSPEDA on the Mag@N1M1 and Mag@N1M3 sorbents is confirmed by the emergence of a nitrogen signal in their EDX spectra, which is absent in the Mag@Me sorbent.

While the amine groups from TMSPEDA contribute hydrophilic character, the overall surface hydrophobicity is tuned by the TMMS and TMSPEDA precursors' ratio, as quantified by the atomic C/N ratio. The C/N ratio for Mag@N1M1 was 9.96, aligning with the theoretical value for its precursors' composition. In contrast, the ratio for Mag@N1M3 increased significantly to 19.05. This progressive change in the C/N ratio provides strong, quantitative support for the varying TMMS and TMSPEDA molar ratios in the Mag@N1M1 and Mag@N1M3 sorbents. The higher C/N ratio indicates a greater abundance of carbon-rich methyl ($-CH_3$) groups on the Mag@N1M3 surface, which directly explains its more hydrophobic character. In addition, the elemental mapping analysis of each element and their combined image approve the uniform distribution of all elements across the material indicating the homogeneousness of the compounds (Fig. 7–9).

The magnetic behaviour of the sorbent materials is a very important issue because it facilitates the extraction of material from the reaction medium and its subsequent reuse. The magnetic susceptibilities of the Fe_3O_4 MNPs, Mag@Me, Mag@N1M1 and Mag@N1M3 compounds were evaluated using VSM instrument. All materials showed excellent magnetic characteristics by indicating no hysteresis in their magnetization curves at ambient temperature which is the characteristic of super-paramagnetic materials (Fig. 10).

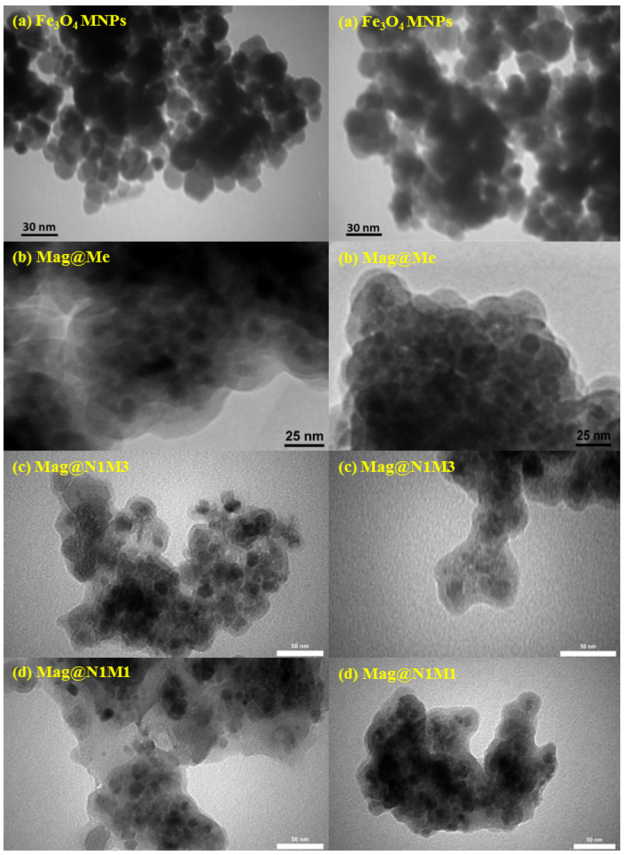

Fig. 6 TEM images of (a) Fe_3O_4 MNPs, (b) Mag@Me, (c) Mag@N1M3, and (d) Mag@N1M1. To see large images, refer to SI.

The saturation magnetizations (Ms) of 66.96, 9.55, 14.62 and 16.09 emu g^{-1} were found for Fe_3O_4, Mag@Me, Mag@N1M3 and Mag@N1M1 compounds, respectively, decreasing from iron oxide to sorbents, in accordance with the further functionalization of magnetic core. The high saturation magnetizations value as well as the super-paramagnetic nature of the prepared adsorbents ensures the high distribution of the sorbent particles in the reaction medium in the absence of magnetic field and at the same time their powerful response to the external magnetic field at the end of process when their complete gathering is requires (as indicated in the inset of Fig. 10).

Thermo-gravimetric analysis is a useful method to explore thermal stability as well as to confirm functional group loading in organic–inorganic hybrid materials. The magnetic sorbent materials were exposed to the TG analysis at the range of RT to 900 °C and the curves are collected in Fig. 11.

As expected, all compounds including Mag@Me, Mag@N1M1 and Mag@N1M3 demonstrated a gradual weight loss with the increasing the temperature owing to decomposition of organic functional groups. On the basis of the TG curves, two main weight losses in all materials could be detected. The first one, at the range of 25–200 °C, could be attributed to the physically and chemically trapped water (or other solvents) in the structure of the materials. The second one, which is a gradual weight loss at the range of 200–600 °C, might be

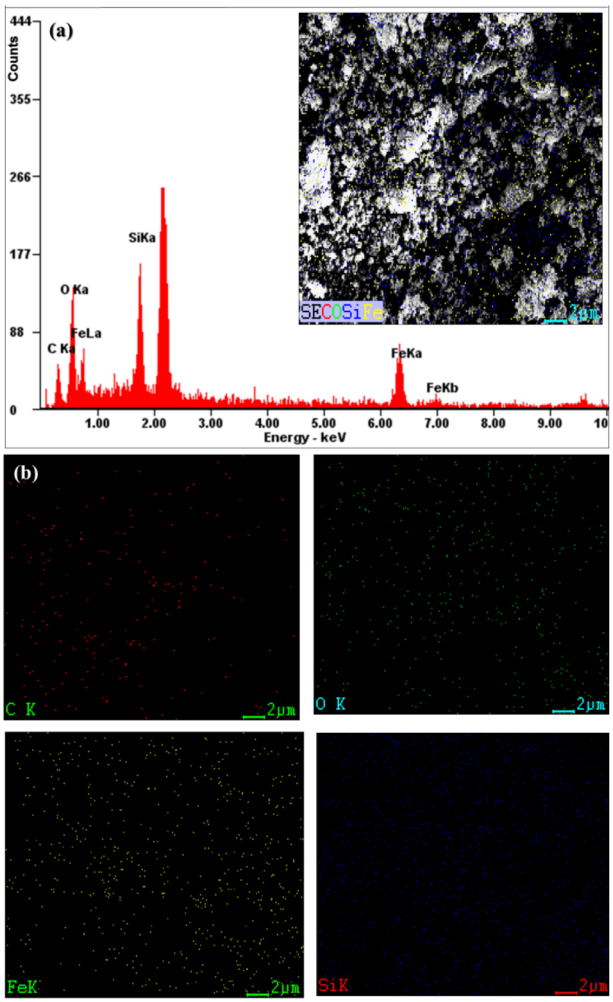

Fig. 7 (a) EDX spectrum and (b) elemental mapping images of Mag@Me sorbent.

related to the decomposition of organic parts of the materials, and is reliable evidence for the successful functionalization of the support with organic moieties. Acceding to the TG curve, we can conclude that the prepared sorbents are thermally stable at least up to 200 °C.

Contact angle measurements were employed to check the hydrophobic or hydrophilic character of the prepared sorbent materials (Fig. 12). To do this, the contact angle of a drop of water with a surface covered with the material was measured. In the case of Mag@Me, the contact angle of 128° was obtained with a drop of water, indicating the relatively high super hydrophobic nature of this compound.

This behaviour is well-match with the incorporation of methyl group on the surface of this material. The same parameter for Mag@N1M3 was found to be 54 and 58° owing to the concomitant existence of TMSPEDA and TMMS on the surface, which resulted in more hydrophilicity compared to Mag@Me. In the Mag@N1M1, with decreasing the ratio of TMMS to TMSPEDA, as expected, due to the more hydrophilic character of its surfaces, the contact angle with a drop of water was decreased to 42 and 45°. Finally, based on the contact angle

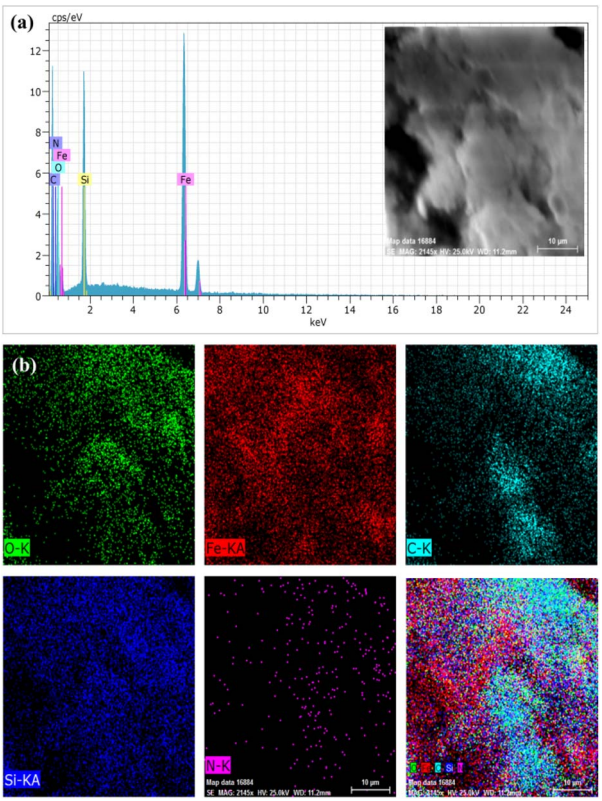

Fig. 8 (a) EDX spectrum and (b) elemental mapping images of Mag@N1M3 sorbent.

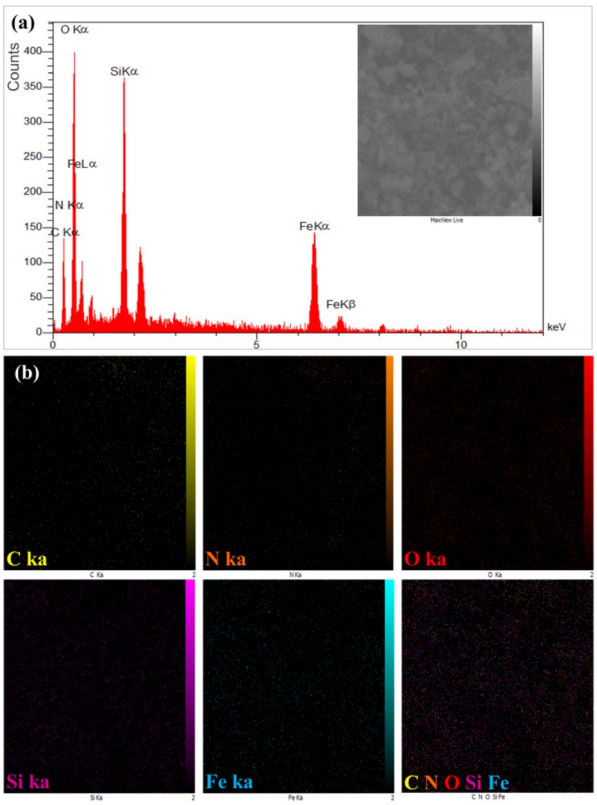

Fig. 9 (a) EDX spectrum and (b) elemental mapping images of Mag@N1M1 sorbent.

data, the order of relative hydrophobicity in the prepared sorbents is as following: Mag@Me > Mag@N1M3 > Mag@N1M1.

Finally, all prepared sorbents demonstrated a typical type IV N_2 adsorption/desorption isotherm, according to the IUPAC categorization, with an H3 hysteresis loop located at the relative pressure of about 0.9, well-matched with the behaviour of nanoparticles in N_2 adsorption/desorption experiments (Fig. S34–S36 in SI). The specific surface area determined using the BET method for the Mag@Me, Mag@N1M1 and Mag@N1M3 materials was found to be 26.1, 19.9 and 34.9 $m^2 g^{-1}$, respectively, which could be attributed to the inter-particle surfaces.

After comprehensive investigations on the structural properties of the prepared sorbents, their capability to separate oil from the oil–water mixtures was evaluated. The separation capacity was determined based on the weight percent of separated oils *via* the formula explained in the experimental part. Accordingly, 0.5 g oil was dispersed in the 40 mL of distilled water and appropriate amounts of the sorbent including Mag@Me, Mag@N1M3 or Mag@N1M1 were added. The treatment time was 7 min. After adsorption of oil by sorbents, the solids were collected using an external magnet and weighed to find adsorption capacity. At first, the ability of sorbents in the separation of used black oil, edible oil and engine oil from water was investigated using 0.1 g of the sorbents. As indicated in Fig. 13, all sorbents demonstrated outstanding ability in separation of the oils from water within 7 min. The maximum and

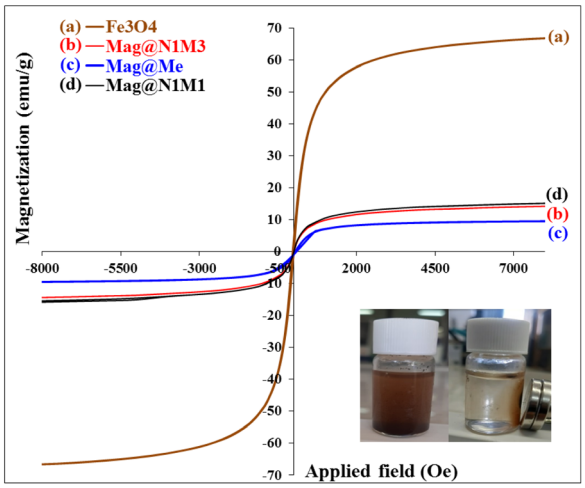

Fig. 10 VSM curves for the (a) Fe_3O_4 (brown curve), (b) Mag@N1M3 (red curve), (c) Mag@Me (blue curve), and (d) Mag@N1M1 (black curve). To see single curves, refer to SI.

minimum efficiency was found for the separation of used black oil by Mag@N1M3 (98.47%) and edible oil by Mag@Me (72.33%), respectively. The removal efficiency of the sorbents in all types of oils was in the following order: Mag@N1M3 > Mag@N1M1 > Mag@Me, which is completely in accordance with the surface character of the prepared materials.

Considering the higher separation capacity of Mag@N1M3, we checked the performance of this material in the oil

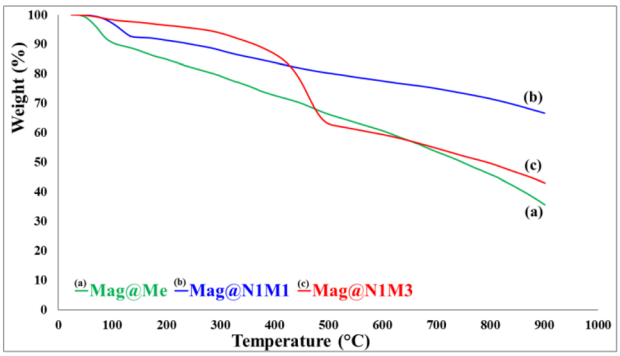

Fig. 11 TGA termograms for (a) Mag@Me, (b) Mag@N1M1, and (c) Mag@N1M3. To see single termograms, refer to SI.

separation using much less amount of sorbent. It was found that by using only 0.07 g of Mag@N1M3 and under other same conditions, the satisfactory separation capacity of 52.2, 65.2 and 65.6% were achieved for the edible oil, engine oil and used black oil, respectively (Fig. 14).

Although these data are reasonable, 0.1 g of the sorbents was employed for the next experiments owing to the much superior results.

Considering the importance of organic pollutant separation from aqueous medium, in the next part of this study, we focused on the separation of *n*-hexane, thinner and toluene from water using the developed magnetic sorbent materials. As can be seen in Fig. 15, good to excellent separation percent was obtained for the separation of all organic pollutants using Mag@Me, Mag@N1M3 and Mag@N1M1 sorbents.

The maximum and minimum efficiency was found for the separation of *n*-hexane by Mag@N1M3 (96.9%) and toluene by Mag@Me (62.3%), respectively.

Additionally, the removal efficiency in all sorbents for various organic pollutants was in the following order: *n*-hexane > thinner > toluene. Similar to the oil separation, the separation capacity of the sorbents in all types of organic pollutant was in the following order: Mag@N1M3 > Mag@N1M1 > Mag@Me. It is assumed that the higher separation capacity of Mag@N1M3 in both oil and organic pollutant separations might be attributed to the balanced hydrophobic/hydrophilic character in its surface, as evidenced by contact angle measurements, which is provides a means of concomitant high dispersion on aqueous media and high interaction of surface with oily compounds.

In other words, with respect to the mechanism of pollutant–sorbent interactions for the removal of oil or non-polar organic pollutants, the main driving force is the hydrophobic interaction. The high density of methyl groups provided by TMMS establishes a hydrophobic surface layer that promotes the transfer of non-polar pollutants from the water phase to the sorbent. As a result, samples with a higher C/N ratio demonstrated a greater affinity for oily/hydrophobic pollutants. In contrast, the adsorption of heavy metals is mainly facilitated by surface complexation. The amine functionalities from TMSPEDA play a key role in this process. This explains why a higher TMSPEDA content was essential for achieving high removal efficiency for Cr pollutant. Therefore, the regulation of

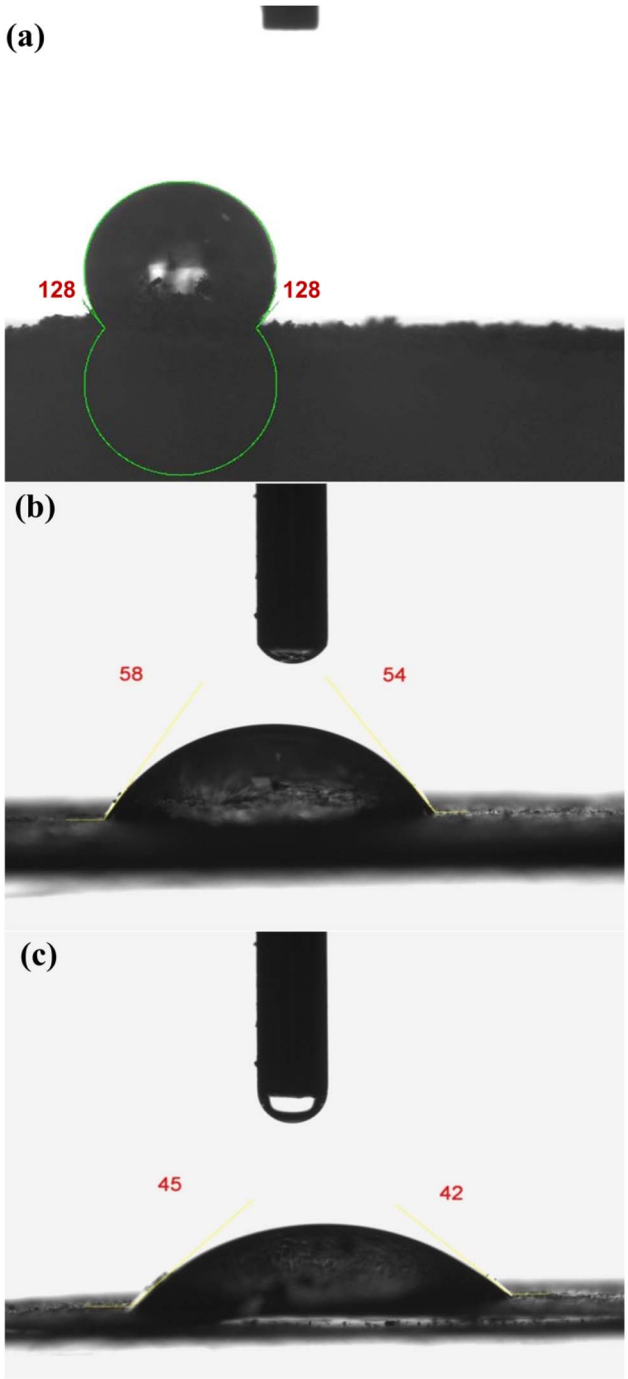

Fig. 12 Contact angle measurements for (a) Mag@Me, (b) Mag@N1M3 and (c) Mag@N1M1.

the TMMS/TMSPEDA ratio on the Mag@Me, Mag@N1M3, and Mag@N1M1 sorbents is not just a synthetic task but an essential method for engineering the surface chemistry of the MNPs. An optimal ratio achieves a dual function with a combination of specific interactions: it provides sufficient hydrophilicity (through TMSPEDA) to ensure stable aqueous dispersion and accessibility to the active sites, while simultaneously incorporating adequate hydrophobicity (through TMMS) to capture non-polar pollutants. This purposeful adjustment of the

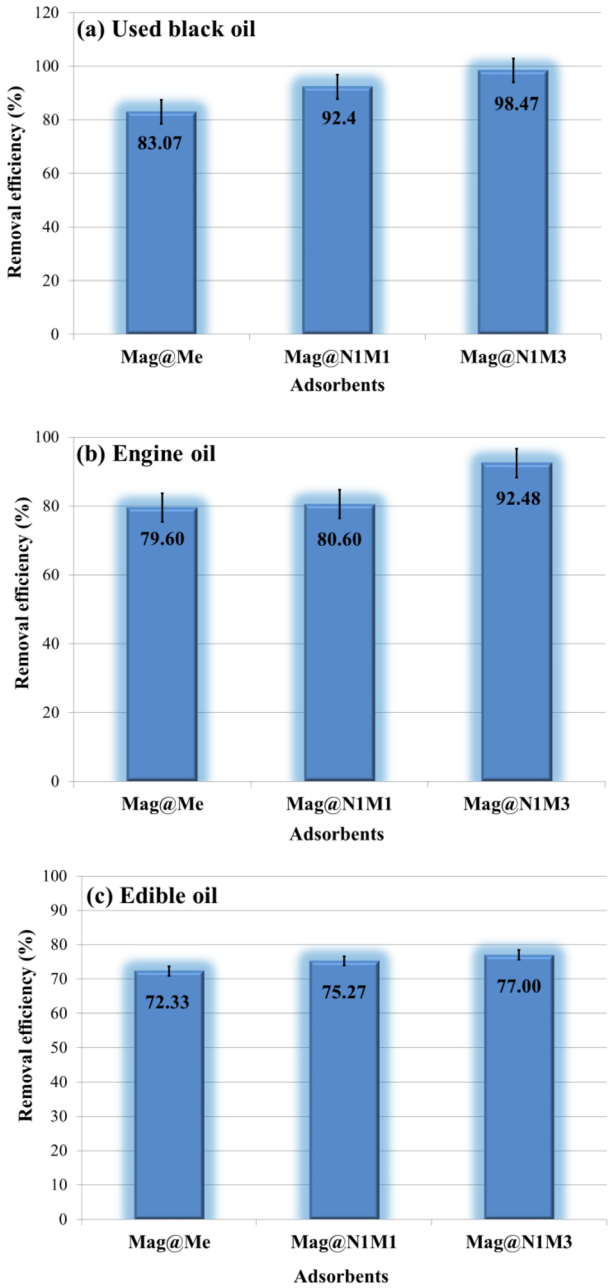

Fig. 13 Removal efficiency (%) of Mag@Me, Mag@N1M3 and Mag@N1M1 sorbents in the separation of (a) used black oil, (b) engine oil, and (c) edible oil from water (using 0.1 g of the sorbents).

hydrophilic–hydrophobic balance allows for the design of task-specific sorbents capable of targeting a wide range of environmental pollutants through unique but complementary mechanisms.

Easy recoverability and reusability of the sorbents is a crucial step forward in the development of green and sustainable sorbent material and is very important from the environmental and economic viewpoints. In the present study, thanks to their high magnetic response, the prepared sorbents could be conveniently separated from the medium only by applying an external magnetic field.

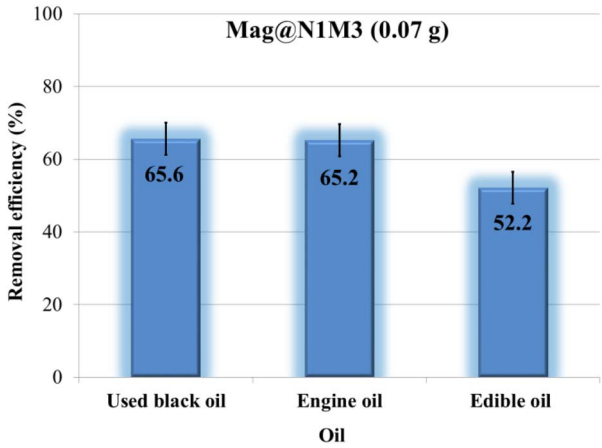

Fig. 14 Removal efficiency (%) of 0.07 g Mag@N1M3 in the separation of used black oil, edible oil and engine oil from water.

Indeed, this simple separation method can enhance the eligibility of the developed sorbents from the practical aspects.

To check the reusability of the system in the separation experiments, after removal of the magnetic sorbents from the medium, they were subjected to acetone for desorption of adsorbed oils or organic pollutants and then dried in oven before reusing in the next runs of separation. The Mag@N1M3 employed for the reusability test owing to its higher performance.

As shown in Fig. 16, the material could be successfully reused for at least 5 consecutive runs in the separation of both oils and organic pollutants with no remarkable loss of removal efficiencies. This excellent reusability could be attributed to the easy as well as complete separation of material from the reaction medium which avoids the loss of sorbent particles during the recovery test. Meanwhile, the tight and strong covalent immobilization of functional groups on the surface of Fe_3O_4@SiO_2 prevents the possibility of leaching of organic moieties as the surface-active adsorption sites and hence improved the recoverability of the system.

Encouraged by the promising results obtained for the separation of both oils and organic pollutants from water using the developed magnetic sorbents, we turned our attention to the ability of the system in the separation of chromium(VI) ion from water, as the next part of this study. Removal of hexavalent chromium from industrial effluents and wastewaters is an important subject in the separation technology since chromium(VI) is dangerous for humans and animals even at low concentrations due to its toxicity and carcinogenic properties.[36–41] A wide variety of sorbents have been applied for the separation of chromium(VI), but development of more effective and task-specific sorbent is still needed. Taking care of these criteria, we explored the capability of as-prepared sorbents in the separation of chromium(VI) at the low concentrations from water. Before, we screened the removal efficacy of chromium(VI) at different times using Mag@N1M1 sorbents to find the optimum time of treatment. As shown in Fig. 17, the removal percent was smoothly enhanced by increasing the time

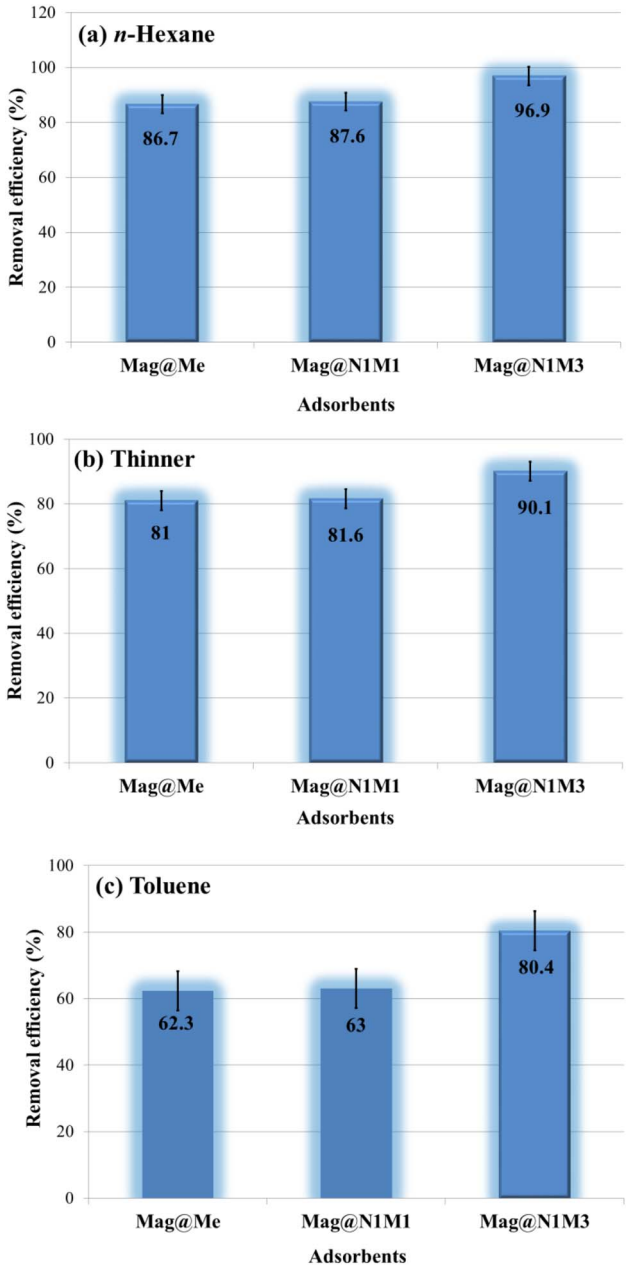

Fig. 15 Removal efficiency (%) of Mag@Me, Mag@N1M3 and Mag@N1M1 sorbents in the separation of (a) *n*-hexane, (b) thinner, and (c) toluene from water (using 0.1 g of the sorbents).

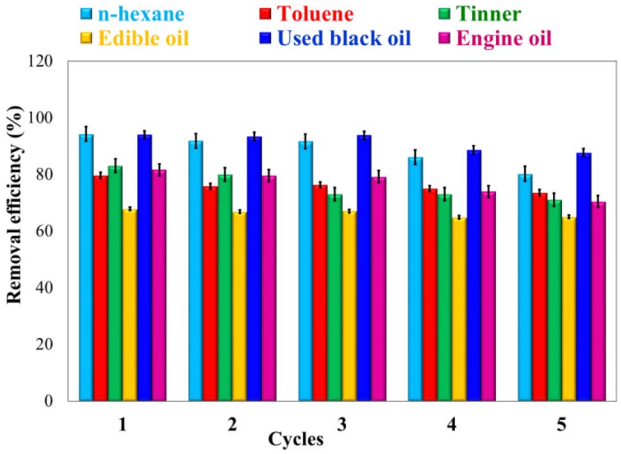

Fig. 16 Reusability of Mag@N1M3 sorbent in the separation of oils and organic pollutants from water.

and reached to the maximum after 120 min. Thus, this time was applied for the next experiments.

Also, to analyze the adsorption of chromium(VI), pseudo-first-order, pseudo-second-order, and intraparticle diffusion kinetic models were applied.[42] The adsorption kinetics were examined by plotting $\ln(q_e - q_t)$ *vs.* t, t/q_t *vs.* t, and q_t *vs.* $t^{0.5}$, as shown in Fig. 17.

The pseudo-first-order rate constant was determined using the plot in Fig. 17a, yielding a $k1$ value of 1.15×10^{-4} and a calculated equilibrium adsorption capacity (q_e) of 34 mg g^{-1}, with an R^2 value of 0.958. The adsorption of chromium(VI) on Mag@N1M1 was further evaluated using the pseudo-second-order model. As demonstrated in Fig. 17b, the data exhibited a fit to the pseudo-second-order model, with an R^2 of 0.9306. Additionally, the applicability of the intraparticle diffusion model was explored as shown in Fig. 17c. Obtained R^2 value was 0.915. Based on these results, the pseudo-first-order kinetic model is the much better model for describing the adsorption of chromium(VI) onto Mag@N1M1 compared to the other models. This indicates that the adsorption process is mainly controlled by physical adsorption and external mass transfer.[43]

Next, the removal efficacy of chromium(VI) at the low concentrations of 2 and 5 mg L^{-1} was investigated using 0.05 g of Mag@Me, Mag@N1M3 and Mag@N1M1 sorbents during 120 min. On the basis of the obtained results, the removal percent was found to be 29, 34.4 and 74.6% at the concentration of 5 mg L^{-1} for the Mag@Me, Mag@N1M3 and Mag@N1M1, respectively (Fig. 18).

Interestingly, the removal efficacies were increased to 35.5, 45 and 83.1%, respectively, when using lower concentration of chromium(VI) (2 mg L^{-1}).

The higher performance of the Mag@N1M1 in the removal of chromium(VI) could be ascribed to the tuned surface functionality as well as higher ratio of TMSPEDA to TMMS which can serve as active nitrogen site for metal ion separation (Fig. 19). FT-IR spectra demonstrate the presence of –NH and $-NH_2$ groups, which become protonated under the experimental conditions, generating positively charged $-NH_3^+$ sites. These protonated amines strongly attract negatively charged Cr(VI) species through electrostatic interactions. Beyond electrostatic attraction, TMSPEDA provides multiple coordination sites that can participate in inner-sphere complexation with Cr(VI). Such multifunctional binding explains the higher adsorption capacity of Mag@N1M1 (33 mg g^{-1}).

Furthermore, the potential leaching of iron from the magnetic sorbents was investigated to assess their stability in aqueous media.

The Mag@N1M1 sorbent was stirred in 10 mL of distilled water for 90 minutes at room temperature. After magnetic separation, the iron content in the solution was analyzed *via* a spectrophotometric method using 1,10-phenanthroline.

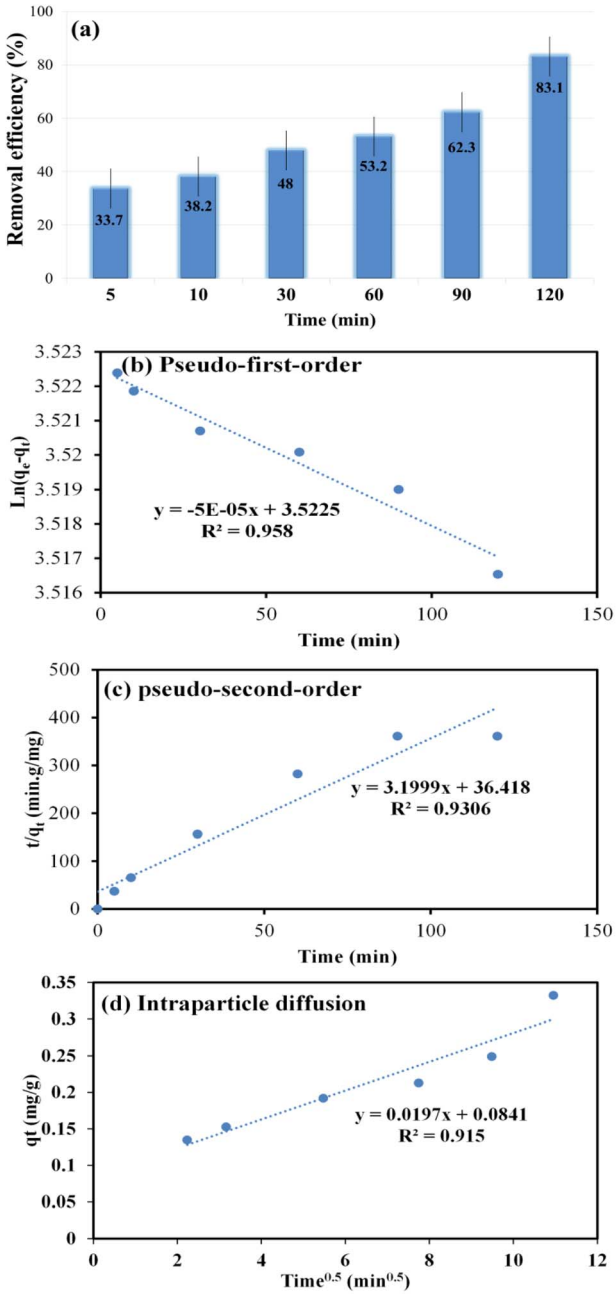

Fig. 17 (a) Removal efficiency (%) of chromium(VI) from a solution with 2 mg L^{-1} concentration using 0.05 g of Mag@N1M1 sorbent at different times and kinetic models for the adsorption of chromium(VI) onto Mag@N1M1: (b) pseudo-first-order model plot ($\ln(q_e - q_t)$ *vs.* t), (c) pseudo-second-order model plot (t/q_t *vs.* t), and (d) intraparticle diffusion model plot (q_t *vs.* $t^{0.5}$). The highest regression coefficient (R^2 = 0.958) for the pseudo-first-order model indicates it is the most suitable, suggesting a physically controlled adsorption process.

Hydroxylamine hydrochloride was added to reduce all Fe^{3+} ions to Fe^{2+}, and 1,10-phenanthroline was then introduced to form an orange–red complex with Fe^{2+}. The pH of the solution was adjusted to 3–4 using ammonium acetate buffer. The absorbance of the iron–phenanthroline complex was measured at 510 nm, and the iron concentration was calculated by

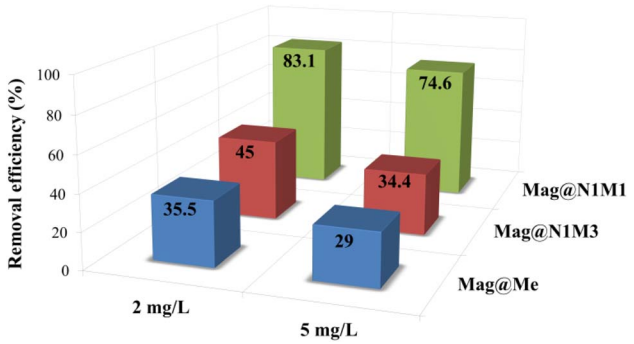

Fig. 18 Removal efficiency (%) of 0.05 g of Mag@Me, Mag@N1M3 and Mag@N1M1 sorbents in the separation of chromium(VI) from water at two concentrations.

comparing the absorbance to a standard calibration curve. Based on the results, the dissolved iron concentration was found to be 0.57 mg L^{-1}. However, in repeated tests, the dissolved iron concentration was significantly lower and undetectable using the spectrophotometric method. This confirms the robust stability of the silica-coated magnetic core and the effectiveness of the functionalization layer in preventing significant iron leaching under the applied conditions.

Furthermore, the adsorption capacity of the Mag@N1M1 sorbent was compared against the adsorption capacity values of different sorbents documented in the literature.[44–49] The findings presented in Table 1 indicate that the Mag@N1M1 sorbent exhibits a good adsorption capacity for eliminating chromium(VI) from aqueous medium, attributed to the large number of nitrogen binding sites on its surfaces (Fig. 19).

Therefore, alongside other sorbents mentioned in the literature, Mag@N1M1 stands out as a promising sorbent for the magnetic extraction of chromium(VI) and various other heavy metals from aqueous medium and industrial wastewater.

While this study demonstrates the high efficacy of the tuned MNPs in simulated laboratory conditions, their performance in complex, real-world water matrices warrants further investigation. Future work will focus on evaluating the sorbent's efficiency and long-term stability using real water samples from various sources to fully assess its potential for practical environmental remediation.

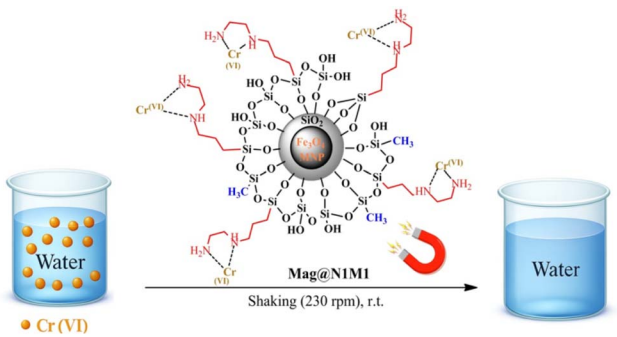

Fig. 19 Schematic of how the removal of chromium(VI) using Mag@N1M1 sorbent.

Table 1 Comparison of the adsorption capacity of Mag@N1M1 sorbent with other magnetic sorbents in eliminating chromium(VI)

Sorbent	Adsorption capacity (mg g^{-1})	Ref.
Surface-modified $MnFe_2O_4$ nanoparticles	31.55	44
Iron–nickel oxide magnetic nanoparticles	30	45
δ-FeOOH-coated maghemite nanoparticles	25.83	46
γ-Fe_2O_3 nanoparticles	19.42	46
SMNPs	26.6	47
Fe_3O_4 hollow microspheres graphene oxide composite	32.33	48
Fe_3O_4 magnetic polymer	32.15	49
Mag@N1M1	33.24	This work

Conclusions

In summary, we developed a highly effective and practical route for the separation of varied oils, organic pollutants and chromium(VI) from aqueous medium *via* targeted functionalization of Fe_3O_4@SiO_2 magnetic nanoparticles with TMMS and/or TMSPEDA using various molar ratios to adapt the hydrophobicity/hydrophilicity of the surface. Among this, Mag@N1M3 demonstrated superior removal efficiencies for the oil removal from water owing to its tuned hydrophobicity/hydrophilicity on the surface. In addition, Mag@N1M1 sorbent was found as the most efficient system for removal of chromium(IV) from water at very low concentrations of 2 mg L^{-1} because of its further coordination sites. Notably, thanks to magnetic behaviour of the prepared sorbents, they could be easily recovered from the reaction mixture by applying an external magnet and successfully reused for at least 5 consecutive runs with no remarkable loss of removal efficiencies. The high removal efficiencies of the prepared sorbents were attributed to the targeted modulation of the surface with task-specific organic moieties which concomitantly facilitates dispersion of the sorbent particles in aqueous medium as well as improved interaction with either oily compounds or metal ion. For practical deployment in treating oil-containing wastewater, the use of these nanosorbents as a polishing step following primary treatments such as gravity separation and coarse filtration is recommended to maximize their efficiency and lifespan. From an economic and practical standpoint, the developed magnetic nanosorbents present a compelling alternative to conventional adsorbents. Unlike single-use materials such as activated carbon or polymeric resins, which require energy-intensive regeneration or disposal, our sorbents are rapidly and completely recovered using a simple magnet, minimizing operational energy consumption and material loss. While the initial cost of silane functionalization is non-negligible, it is substantially amortized over multiple uses, as demonstrated by the consistent performance over five consecutive cycles. This reusability, combined with their dual-functionality for both oils and heavy metals, offers a more sustainable and potentially cost-effective lifecycle compared with many specialized adsorbents that target only a single pollutant class. Furthermore, the synthesis avoids expensive or rare materials, relying on an iron oxide core and a scalable coating process. These attributes collectively suggest a strong potential for reducing long-term operational costs in practical water remediation situations.

Author contributions

A. M.: supervision, conceptualization, validation, methodology, formal analysis, resources, writing – original draft, writing – review and editing; H. P.: formal analysis, investigation, data curation; M. Sh.: supervision, validation, conceptualization, formal analysis, resources; F. M.: formal analysis, validation, writing – review and editing. All authors have read and agreed to the published version of the manuscript.

Conflicts of interest

There are no conflicts to declare.

Data availability

All required data supporting the findings are available in the manuscript and its supplementary information (SI). If the readers require any additional data, the authors will provide it in electronic format upon reasonable request. Supplementary information is available. See DOI: https://doi.org/10.1039/d5ra06301a.

Acknowledgements

The authors greatly acknowledge the Kharazmi University research council for financial support of this work. This work is based upon research funded by Iran National Science Foundation (INSF) under project no. 4043659.

References

1 J. Coleman, J. Baker, C. Cooper, M. Fingas, G. Hunt, K. Kvenvolden, K. Michel, J. Michel, J. Mcdowell, J. Phinney, R. Pond, R. Rabalais, L. Roesner and R. B. Spies, Oil in the Sea III, in *National Academy of Science*, Washington, DC, 2003, p. 16.
2 B. Bhushan, Bioinspired oil–water separation approaches for oil spill clean-up and water purification, *Philos. Trans. R. Soc.*, 2019, **A 377**, 20190120.

3 N. Bhardwaj and A. N. Bhaskarwar, A review on sorbent devices for oil-spill control, *Environ. Pollut.*, 2018, **243**, 1758.
4 F. Wang, Sh. Lei, J. Ou, Ch. Li and W. Li, Novel all-natural material for oil/water separation, *Ind. Eng. Chem. Res.*, 2019, **58**, 1924.
5 Zh. Lian, J. Xu, Z. Wang, Zh. Yu, W. Zh and H. Yu, Nanosecond laser-induced underwater superoleophobic and under oil superhydrophobic mesh for oil/water separation, *Langmuir*, 2018, **34**, 2981.
6 T. Zhang, Zh. Li, Y. Lü, Y. Liu, D. Yang, Q. Li and F. Qiu, Recent progress and future prospects of oil-absorbing materials, *Chin. J. Chem. Eng.*, 2019, **27**, 1282.
7 J. Ge, H. Y. Zhao, H. W. Zhu, J. Huang, L. A. Shi and Sh. H. Yu, Advanced sorbents for oil-spill cleanup: recent advances and future perspectives, *Adv. Mater.*, 2016, **28**, 10459.
8 Y. Yang, X. Jiang, Kh. L. Goh and K. Wang, The separation of oily water using low-cost natural materials: review and development, *Chemosphere*, 2021, **285**, 131398.
9 J. Yong, J. Huo, F. Chen, Q. Yang and X. Hou, Oil/water separation based on natural materials with super-wettability: recent advances, *Phys. Chem. Chem. Phys.*, 2018, **20**, 25140.
10 A. T. Hoang, X. Ph. Nguyen, X. Q. Duong and Th. T. Huynh, Sorbent-based devices for the removal of spilled oil from water: a review, *Environ. Sci. Pollut. Res.*, 2021, **28**, 28876.
11 M. Shahmirzaee, J. Abdi, A. Hemmati-Sarapardeh, M. Schaffie, M. Ranjbar and A. Khataee, Metal-organic frameworks as advanced sorbents for oil/water separation, *J. Mol. Liq.*, 2022, **363**, 119900.
12 A. M. Abudayyeh, L. A. M. Mahmoud, V. P. Ting and S. Nayak, Metal–organic frameworks (MOFs) and their composites for oil/water separation, *ACS Omega*, 2024, **9**, 47374.
13 B. Wan, Sh. Feng, C. Wang, X. Liu, L. Chen and D. Yan, Nanostructure-based oil–water separation: mechanism and status, *Separations*, 2023, **10**, 569.
14 N. Y. Abu-Thabit, O. J. Uwaezuoke and M. H. A. Elella, Superhydrophobic nanohybrid sponges for separation of oil/water mixtures, *Chemosphere*, 2022, **294**, 133644.
15 S. M. Hailan, I. Krupa and G. McKay, Removal of oil spills from aqueous systems by polymer sorbents, *Int. J. Environ. Sci. Technol.*, 2025, **22**, 3833.
16 M. Fouladi, M. K. Heidari and O. Tavakoli, Development of porous biodegradable sorbents for oil/water separation: a critical review, *J. Porous Mater.*, 2023, **30**, 1037.
17 B. Wang, W. Liang, Zh. Guo and W. Liu, Biomimetic super-lyophobic and super-lyophilic materials applied for oil/water separation: a new strategy beyond nature, *Chem. Soc. Rev.*, 2015, **44**, 336.
18 A. O. Ifelebuegu and A. Johnson, Nonconventional low-cost cellulose- and keratin-based biopolymeric sorbents for oil/water separation and spill cleanup: a review, *Crit. Rev. Environ. Sci. Technol.*, 2017, **47**, 964.
19 Zh. Xue, Y. Cao, N. Liu, L. Feng and L. Jiang, Special wettable materials for oil/water separation, *J. Mater. Chem. A*, 2014, **2**, 2445.
20 Y. Wang, Ch. You, C. Kowall, L. Li and A. Nanometer-thick, mechanically robust, and easy-to-fabricate simultaneously oleophobic/hydrophilic polymer coating for oil-water separation, *Ind. Eng. Chem. Res.*, 2018, **57**, 15395.
21 (*a*) S. Pervaiz, M. Javed, A. Shah, A. Latif, S. Nasird and I. Shah, *RSC Adv.*, 2025, **15**, 19899; (*b*) J. Ma, H. Wang, M. Zhang, D. Li, L. Liua and H. Yang, Preparation of terpyridine-functionalized paramagnetic nickel–zinc ferrite microspheres for adsorbing Pb(II), Hg(II), and Cd(II) from water, *RSC Adv.*, 2020, **10**, 39468.
22 (*a*) M. Moradi-Bieranvand, S. Farhadi, A. Zabardasti and F. Mahmoudi, Construction of magnetic MoS_2/$NiFe_2O_4$/MIL-101(Fe) hybrid nanostructures for separation of dyes and antibiotics from aqueous media, *RSC Adv.*, 2024, **14**, 11037; (*b*) G. Simonsen, M. Strand and G. Øye, Potential applications of magnetic nanoparticles within separation in the petroleum industry, *J. Pet. Sci. Eng.*, 2018, **165**, 488.
23 S. Mirshahghassemi and J. R. Lead, Oil recovery from water under environmentally relevant conditions using magnetic nanoparticles, *Environ. Sci. Technol.*, 2015, **49**, 11729.
24 T. Yousofi and A. Rahmati, Fe_3O_4@SiO_2-BU core-shell as a new nanomagnetic gelator for oil recovery from water, *Polyhedron*, 2020, **180**, 114363.
25 S. Zhang, T. Lü, D. Qi, Z. Cao, D. Zhang and H. Zhao, Synthesis of quaternized chitosan-coated magnetic nanoparticles for oil-water separation, *Mater. Lett.*, 2017, **191**, 128.
26 W. F. Elmobarak and F. Almomani, A new insight into the separation of oil from oil/water emulsion by Fe_3O_4-SiO_2 nanoparticles, *Environ. Res.*, 2021, **202**, 111645.
27 L. Yu, G. Hao, J. Gu, S. Zhou, N. Zhang and W. Jiang, Fe_3O_4/PS magnetic nanoparticles: synthesis, characterization and their application as sorbents of oil from waste water, *J. Magn. Magn. Mater.*, 2015, **394**, 14.
28 R. Sun, L. He, Q. Shang, Sh. Jiang, Ch. Zhou, P. Hong, H. Zhao, Sh. Sun and Ch. Li, Hydrophobic magnetic porous material of Eichhornia crassipes for highly efficient oil adsorption and separation, *ACS Omega*, 2020, **5**, 9920.
29 Y. Zhai and X. Yuan, Superhydrophobic, magnetic aerogels based on nanocellulose fibers derived from harakeke for oily Wastewater Remediation, *Polymers*, 2023, **15**, 3941.
30 M. Alimohammadian, S. Azizian and B. Sohrabi, Preparation of the graphene-based smart hydrophobic nanocomposite and its application in oil/water separation, *Sci. Rep.*, 2023, **13**, 19816.
31 M. Farahat, A. Sobhy and M. M. S. Sanad, Superhydrophobic magnetic sorbent *via* surface modification of banded iron formation for oily water treatment, *Sci. Rep.*, 2022, **12**, 11016.
32 H. Wu, L. Hao, Ch. Chen and J. Zhou, Superhydrophobic Fe_3O_4/OA magnetorheological fluid for removing oil slick from water surfaces effectively and quickly, *ACS Omega*, 2020, **5**, 27425.
33 A. Mobaraki, B. Movassagh and B. Karimi, Hydrophobicity-enhanced magnetic solid sulfonic acid: a simple approach to improve the mass transfer of reaction partners on the surface of the heterogeneous catalyst in water-generating reactions, *Appl. Catal., A*, 2014, **472**, 123.

34 A. Mobaraki, N. Sakhaee, A. Takallou and A. Habibi, Triple action of an attractive deep eutectic solvent in the synthesis of aryl nitriles and substituted triazoles using a magnetically reusable Fe_3O_4@SiO_2@PrNCu Catalyst, *ChemistrySelect*, 2023, **8**, e202204932.

35 A. Mobaraki, M. Hajibeygi, H. Moradi, M. Pirasteh and A. Takallou, Design of an efficient magnetic brush solid acid and its catalytic use in organic reactions, *Sci. Rep.*, 2025, **15**, 2828.

36 (*a*) L. Yin, K. Wang, L. Jiang, Y. Xi, Z. Xu, Z. Song and H. Zhou, Green synthesis and adsorption performance of Fe_3O_4/chitosan/polypyrrole composites for efficient removal of chromium ion, *RSC Adv.*, 2025, **15**, 16337; (*b*) Zh. Jiang, K. Chen, Y. Zhang, Y. Wang, F. Wang, G. Zhang and D. D. Dionysiou, Magnetically recoverable $MgFe_2O_4$/conjugated polyvinyl chloride derivative nanocomposite with higher visible-light photocatalytic activity for treating Cr(VI)-polluted water, *Sep. Purif. Technol.*, 2020, **236**, 116272.

37 R. Acharya, A. Lenka and K. Parida, Magnetite modified amino group based polymer nanocomposites towards efficient adsorptive detoxification of aqueous Cr (VI): a review, *J. Mol. Liq.*, 2021, **337**, 116487.

38 N. Nahurskyi, M. Malovany, I. Bordun and E. Szymczykiewicz, Magnetically sensitive carbon-based nanocomposites for the removal of dyes and heavy metals from wastewater: a review, *Chem. Chem. Technol.*, 2024, **18**, 170.

39 M. K. Goswami, A. Srivastava, R. K. Dohare, A. K. Tiwari and A. Srivastav, Recent advances in conducting polymer-based magnetic nanosorbents for dyes and heavy metal removal: fabrication, applications, and perspective, *Environ. Sci. Pollut. Res.*, 2023, **30**, 73031.

40 W. Cai, F. Fu, L. Zhu and B. Tang, Simultaneous removal of chromium(VI) and phosphate from water using easily separable magnetite/pyrite nanocomposite, *J. Alloys Compd.*, 2019, **803**, 118.

41 H. P. Nogueira, S. H. Toma, A. T. Silveira, A. A. C. Carvalho, A. M. Fioroto and K. Araki, Efficient Cr(VI) removal from wastewater by activated carbon superparamagnetic composites, *Microchem. J.*, 2019, **149**, 104025.

42 S. Aber and M. Sheydaei, Removal of COD from industrial effluent containing indigo dye using adsorption method by activated carbon cloth: optimization, kinetic, and isotherm studies, *Clean:Soil, Air, Water*, 2012, **40**, 87.

43 Y. S. Chang, P. I. Au, N. M. Mubarak, M. Khalid, P. Jagadish, R. Walvekar and E. C. Abdullah, Adsorption of Cu (II) and Ni (II) ions from wastewater onto bentonite and bentonite/GO composite, *Environ. Sci. Pollut. Res.*, 2020, **27**, 33270.

44 J. Hu, I. M. C. Lo and G. Chen, Fast removal and recovery of Cr(VI) using surface modified Jacobsite ($MnFe_2O_4$) nanoparticles, *Langmuir*, 2005, **21**, 11173.

45 L. Wei, G. Yang, R. Wang and W. Ma, Selective adsorption and separation of chromium (VI) on the magnetic iron-nickel oxide from waste nickel liquid, *J. Hazard. Mater.*, 2009, **164**, 1159.

46 J. Hu, I. M. C. Lo and G. Chen, Performance and mechanism of chromate (VI) adsorption by δ-FeOOH-coated maghemite (γ-Fe_2O_3) nanoparticles, *Sep. Purif. Technol.*, 2007, **58**, 76.

47 P. N. Singh, D. Tiwary and I. Sinha, Starch-functionalized magnetite nanoparticles for hexavalent chromium removal from aqueous solutions, *Desalin. Water Treat.*, 2016, **57**, 12608.

48 M. Liu, T. Wen, X. Wu, C. Chen, J. Hu, J. Li and X. Wang, Synthesis of porous Fe_3O_4 hollow microspheres/graphene oxide composite for Cr(VI) removal, *Dalton Trans.*, 2013, **42**, 14710.

49 Y. G. Zhao, H. Y. Shen, S. D. Pan and M. Q. Hu, Synthesis, characterization and properties of ethylenediamine-functionalized Fe_3O_4 magnetic polymers for removal of Cr(VI) in wastewater, *J. Hazard. Mater.*, 2010, **182**, 295.